New mesh-type phantoms and their dosimetry applications including emergencies

C.H. Kim[a], Y.S. Yeom[a], T.T. Nguyen[a], M.C. Han[a], C. Choi[a], H. Lee[a], H. Han[a], B. Shin[a], J.-K. Lee[a], H.S. Kim[b], M. Zankl[c], N. Petoussi-Henss[d], W.E. Bolch[e], C. Lee[f], B.S. Chung[g], R. Qiu[h], K. Eckerman[i]

[a] *Department of Nuclear Engineering, Hanyang University, 04763, 222 Wangsimni-ro, Seongdong-gu, Seoul, Republic of Korea; e-mail: chkim@hanyang.ac.kr*

[b] *National Radiation Emergency Medical Center, Korea Institute of Radiological & Medical Sciences (KIRAMS), 01812, 75 Nowon-ro, Nowon-gu, Seoul, Republic of Korea; e-mail: hskim87@kirams.re.kr*

[c] *Research Unit Medical Radiation Physics and Diagnostics, Helmholtz Zentrum München Deutsches Forschungszentrum für Gesundheit und Umwelt (GmbH), Ingolstädter Landstraße 1, D-85764 Neuherberg, Germany; e-mail: zankl@helmholtz-muenchen.de*

[d] *Research Unit Medical Radiation Physics and Diagnostics, Helmholtz Zentrum München Deutsches Forschungszentrum für Gesundheit und Umwelt (GmbH), Ingolstädter Landstraße 1, D-85764 Neuherberg, Germany; e-mail: petoussi@helmholtz-muenchen.de*

[e] *J. Crayton Pruitt Family Department of Biomedical Engineering, University of Florida, P.O. Box 116131, Gainesville, FL 32611-6131, USA; e-mail: wbolch@ufl.edu*

[f] *Division of Cancer Epidemiology & Genetics, National Cancer Institute, 9609 Medical Center Drive, Bethesda, MD 20892-9760, USA; e-mail: leechoonsik@mail.nih.gov*

[g] *Department of Anatomy, Ajou University School of Medicine, 16499, 206 Worldcup-ro, Suwon, Republic of Korea; e-mail: bschung@ajou.ac.kr*

[h] *Department of Engineering Physics, Tsinghua University, 100084, P.R. China; e-mail: qiurui@tsinghua.edu.cn*

[i] *Environmental Sciences Division, Oak Ridge National Laboratory, Oak Ridge, TN 37831-6480 USA; e-mail: eckermankf@ornl.gov*

Abstract–Mesh-type adult reference computational phantoms have been constructed within Committee 2 of the International Commission on Radiological Protection (ICRP) through the conversion of the voxel-type *Publication* 110 adult reference computational phantoms to a high-quality mesh format. Furthermore, various radiosensitive tissue layers were added that were below the image resolution of the voxel phantoms and therefore not included within the *Publication* 110 phantoms. The new mesh phantoms include all necessary source and target tissues for computing the effective dose, including the 8 to 40-μm-thick radiosensitive target layers of the alimentary and respiratory tract organs, thereby obviating the need for supplemental stylised models (e.g. respiratory airways, alimentary tract organ walls and stem cell layers, lens of the eye and skin basal layer). To see the impact of the new mesh-type reference phantoms, dose coefficients for some selected external and internal exposures were calculated and compared to reference values given in *Publications* 116 and 133 which were calculated by employing the *Publication* 110 phantoms and the supplemental stylised models. The new mesh phantoms were also used to calculate dose coefficients for industrial radiography sources near the body, which can be used to estimate the organ doses of the worker who is accidently exposed by an industrial radiography source; in these calculations, the mesh phantoms were deformed to reflect the size of the worker and also to evaluate the effect of the posture on the magnitude of the dose coefficients.

Keywords: Reference phantom; Voxel; Mesh; Monte Carlo; Dose coefficient

1. INTRODUCTION

Following the issuance of the 2007 Recommendations of the International Commission on Radiological Protection (ICRP) (ICRP, 2007), the Commission released the ICRP adult reference computational phantoms with *Publication* 110 (ICRP, 2009). These *Publication* 110 reference phantoms are voxel-type computational phantoms constructed from whole-body computed tomography (CT) data of adult male and female patient. They are consistent with the information in *Publication* 89 (ICRP, 2002), the reference anatomical parameters of

Reference Adult Male and Reference Adult Female. The voxel-type *Publication* 110 reference phantoms have been used to produce reference dose coefficients of equivalent and effective doses for external and internal exposures, following the current ICRP dosimetric framework (ICRP, 2010, 2015, 2016, 2017).

While providing anatomically more realistic representations of the human body than the first-generation computational phantoms (i.e. stylised or mathematical phantoms), the voxel-type *Publication* 110 reference phantoms, due to millimetre-scale voxel resolutions (male: 2.137 × 2.137 × 8 mm^3, female: 1.775 × 1.775 × 4.8 mm^3), do not include small or thin tissues, particularly micron-scale radiosensitive target layers (e.g., the stem cell layers of respiratory and alimentary tract organs and the skin basal layer), eventually leading to limitations in dose coefficient (DC) calculations for weakly penetrating radiations (i.e., low-energy photons and charged particles). Therefore, several supplemental organ-specific stylised models were developed and used for separate simulations to calculate reference DCs for some exposure cases, for which the *Publication* 110 phantoms do not provide reliable dose values (ICRP, 2010, 2015, 2016, 2017). In addition, due to the nature of voxel geometry, it is very difficult, if not impossible, to deform the *Publication* 110 reference phantoms into different body sizes or postures, which is needed for personalization of dose calculations in emergency or accident exposure situations.

Acknowledging these limitations, the Commission has recently launched a new Task Group (i.e. Task Group 103) under Committee 2 with the aim of developing new mesh-type reference computational phantoms (MRCPs) by converting the current voxel-type reference phantoms into a high-quality mesh format. Note that these mesh-type phantoms, represented by polygon mesh (PM) or tetrahedron mesh (TM) as necessary, are considered at the present as an advanced type of computational phantoms that can be directly implemented into Monte Carlo codes, i.e. without voxelization, fully maintaining the advantages of the mesh geometry over the voxel geometry in Monte Carlo dose calculations (Kim et al., 2011; Han et al., 2013; Yeom et al., 2013; Yeom et al., 2014; Han et al., 2015). Very recently, Task Group 103 has completed the development of the MRCPs for adult male and female, converted from the voxel-type *Publication* 110 reference phantoms (Nguyen et al., 2015; Kim et al., 2016; Yeom et al., 2016a; Yeom et al., 2016b; Kim et al., 2017).

This paper introduces the new adult MRCPs, with a brief explanation of the development process, and discusses their compatibility with some major general-purpose Monte Carlo codes and the impact on dose coefficient calculations. In addition, the first application of the MRCPs by Task Group 103 is explained, which is the calculation of dose coefficients for industrial radiography sources for use in dose estimation of workers who are accidently exposed to an industrial radiography source.

2. ADULT MESH-TYPE REFERENCE PHANTOMS

Most of the organs and tissues of the adult MRCPs were constructed by directly converting the voxel-type *Publication* 110 reference phantoms into mesh format through 3D surface rending and several refinement procedures (Kim et al., 2016). During the conversion process, the shape of each organ/tissue of the mesh model was matched to the voxel model, maximizing the geometric similarity between two objects, which was monitored by Dice index (DI) (Dice, 1945) and centroid distance (CD). The direct conversion method was also used to construct the bones, except for some bones such as the spine, hand and foot bones which were constructed from existing high-quality mesh models by morphing, again

monitoring the DI and CD. Detailed information on the construction of the skeletal system can be found elsewhere (Yeom et al., 2016b).

Several organs and tissues (e.g. small intestine, lymphatic nodes, eye and blood in large vessels), which are very complex and/or small in structure, could not be produced by the conversion process; therefore, they were modelled. The small intestine of each phantom was generated by using a dedicated procedure and a computer program developed by Yeom et al. (2016a), in which a total of 1000 different models of the small intestine are randomly generated with a Monte Carlo approach and then the best model is selected considering both geometric and dosimetric similarity. The lymphatic nodes were generated by using a similar approach which was used to generate the lymphatic nodes in the UF/NCI adult phantoms (Lee et al., 2013), based on the lymphatic node data in *Publication* 133 (ICRP, 2016). The detailed eye model, which was developed by Behrens et al. (2009) and adopted to calculate the lens dose coefficients (DCs) in *Publication* 116 (ICRP 2010), was reproduced in high-quality mesh format and installed in the MRCPs (Nguyen et al., 2015). The blood in the large vessels (Fig. 1) was modelled considering both the distribution of the blood in the voxel phantoms and the shape of the 3D blood models in BioDigital (https://www.biodigital.com) and also matching the mass to the reference masses given in *Publication* 89 (ICRP, 2004). The constructed models were finally reviewed and confirmed by an anatomist.

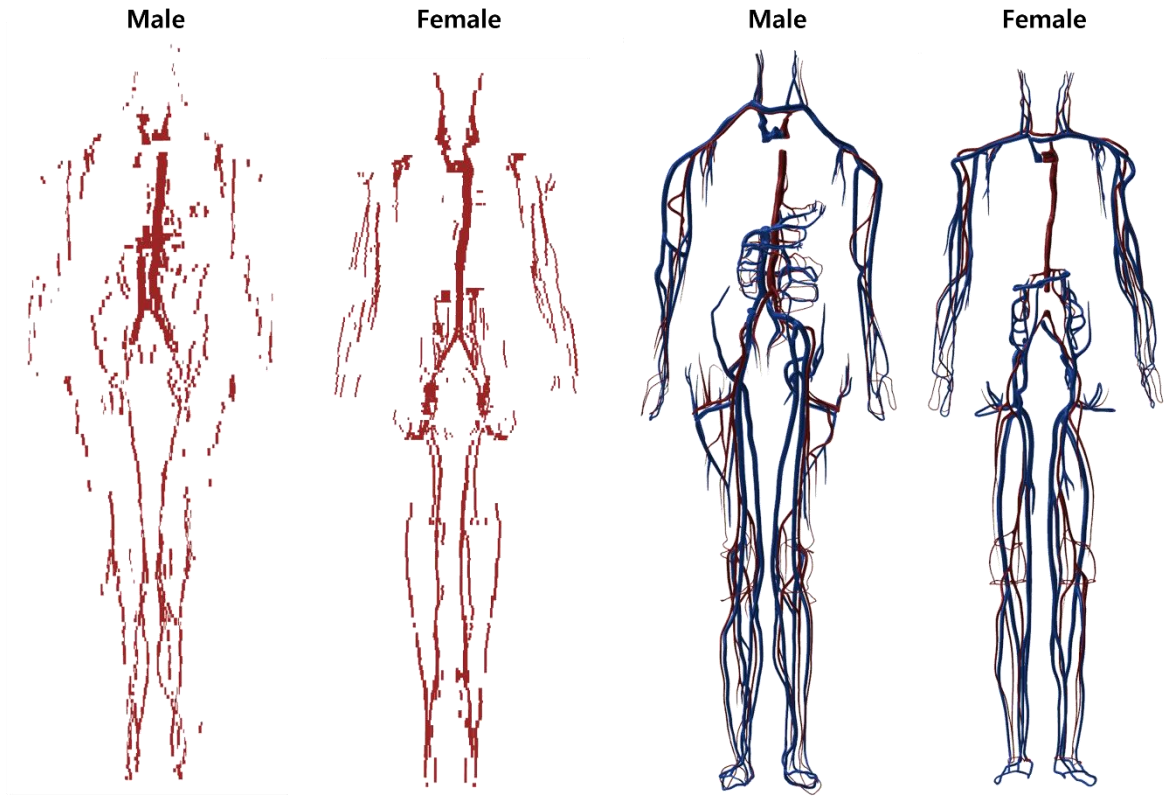

Fig. 1. Blood in large vessels of the *Publication* 110 phantoms (left) and the MRCPs (right). In the MRCPs, the red colour indicates the blood in the large arteries and the blue colour indicates the blood in the large veins.

The *Publication* 110 phantoms (ICRP, 2009), as well as the other previous computational phantoms (Kramer et al., 1982; Zankl et al., 2005; Kramer et al., 2006; Lee et al., 2007; Zhang et al., 2009; Lee et al., 2010; Yeom et al., 2013), were matched to the reference organ/tissue masses listed in Table 2.8 of *Publication* 89 (ICRP, 2002), which are the parenchyma masses of the organs and tissues, i.e. not including blood content. It is true that a

large portion of blood situated in the small vessels and capillaries is distributed in the organs and tissues; therefore, the MRCPs were adjusted to the organ/tissue masses and compositions which are inclusive of the blood content. For this, the organ/tissue masses and compositions were recalculated following the reference regional blood volume fractions in *Publication* 89 (ICRP, 2002). Note that a similar approach has been used for the calculation of SAFs for the self-irradiation cases in *Publication* 133 (ICRP, 2016).

Micron-thick target and source regions of the skin and alimentary and respiratory tract organs were included in the MRCPs. The 50-μm-thick skin basal cell layer (i.e. 50 to 100 μm below the skin surface), is considered appropriate for specifying the sensitive layer (ICRP, 1977, 2010, 2015), was defined in the MRCPs, as shown in Fig. 2, simply by using the *Offset* function that shrinks or enlarges a polygon-mesh surface in the normal directions of the facets in the surface, which allows the creation of surfaces to define the tens-of-micrometre-thick layer at a specific depth. Likewise, the thin target and source regions of the alimentary tract organs (oral cavity, oesophagus, stomach, small intestine and large intestine) and the respiratory tract organs (extrathoracic region, bronchi, bronchiole and alveoli-interstitial region) were defined in the MRCPs, following the morphometric data given in *Publications* 66 and 100 (ICRP, 1994, 2006). Detailed lung airway models to represent the bronchi and bronchioles were also developed using the branch generation algorithm of Tawhai et al. (2000), as shown in Fig. 3. More detailed information on the alimentary and respiratory tract system can be found elsewhere (Kim et al., 2017).

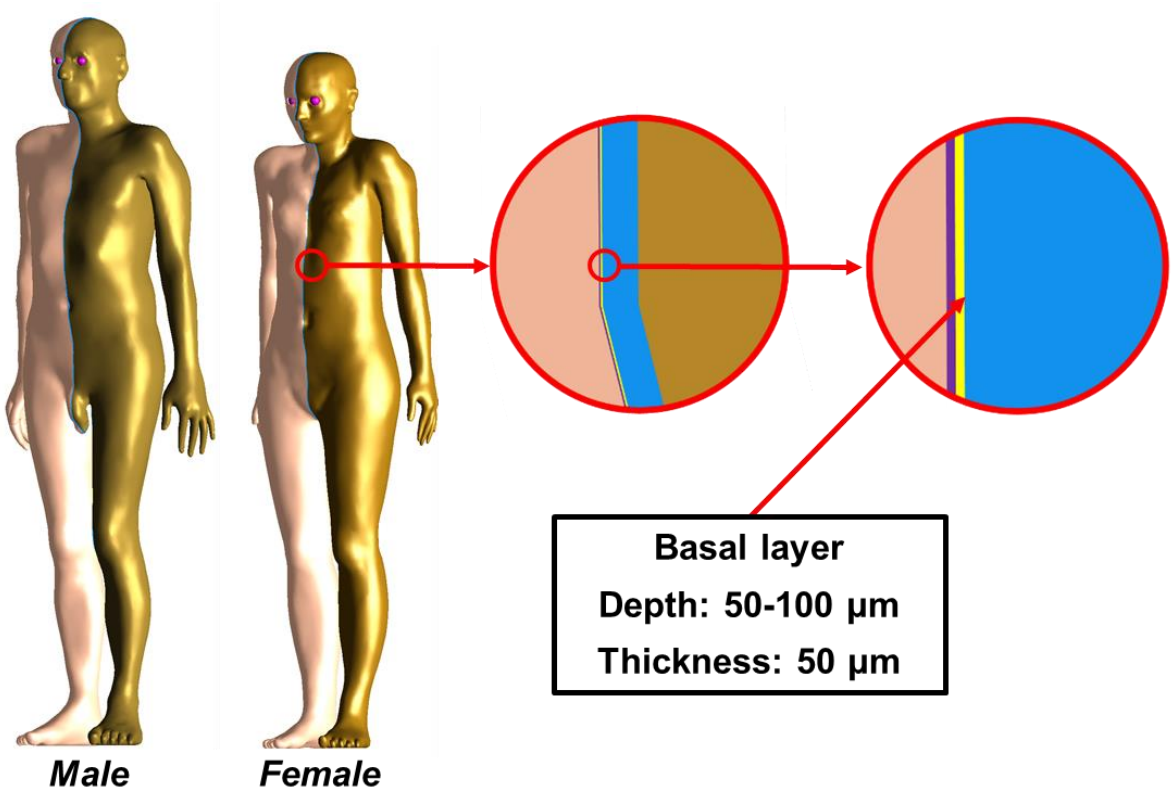

Fig. 2. Skin of the adult MRCPs including the 50-μm-thick target layer: dead layer (purple), target layer (yellow) and dermis layer (blue).

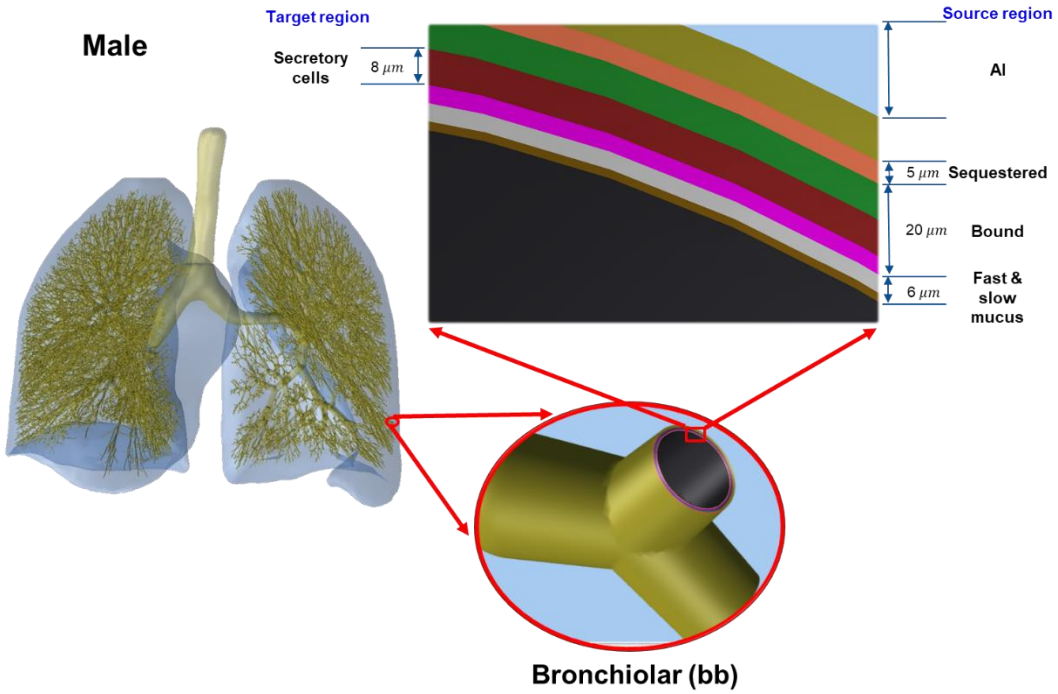

Fig. 3. Detailed airway model incorporated in the lungs of the adult male MRCP (Kim et al., 2017).

Fig. 4 shows the adult male and female MRCPs, along with the voxel-type *Publication* 110 reference phantoms. The body height and weight of the MRCPs exactly match the reference values (male: 176 cm and 73 kg; female: 163 cm and 60 kg). The masses of the organs and tissues of the MRCPs match the reference values, inclusive of blood content, within 0.1% of difference. The male MRCP is composed of 2.5 million triangular facets in the polygon-mesh (PM) format and 8.2 million tetrahedrons in the tetrahedron-mesh (TM) format. The female MRCP is composed of 2.6 million triangular facets in the PM format and 8.6 million tetrahedrons in the TM format. Note that the TM-version MRCPs were directly converted from the PM-version MRCPs without any geometric distortion, by using the TetGen code (Si, 2015). The MRCPs include all the radiosensitive organs and tissues relevant to the dose assessment for ionizing radiation exposure for radiological protection purpose, thereby completely obviating the need for supplemental stylised models such as respiratory airways, alimentary tract organ walls and stem cell layers, lens of the eye and skin basal cell layer. The red bone marrow (RBM) and endosteum are not explicitly modelled in the MRCPs and the doses to these tissues need to be estimated by using the skeletal-dose-calculation methods (e.g. fluence-to-dose response functions), as in *Publication* 116 (ICRP, 2010). Note that the lung airway models, representing bronchi (BB) and bronchioles (bb), were produced in the constructive solid geometry (CSG) format, not in mesh format, and can be installed in the MRCPs, as necessary, using the Geant4 code via the parallel-geometry technique (Apostolakis et al., 2008; Kim et al., 2017). The MRCPs have overcome the geometrical limitations of the *Publication* 110 phantoms due to the limited voxel resolutions and the nature of voxel geometry. For example, as shown in Fig. 4, the *Publication* 110 phantoms show stair-stepped surfaces of the organs and tissues, whereas the MRCPs show smooth surfaces. In addition, all the organs and tissues in the thin structure (e.g. skin, gastrointestinal (GI) tract organs and cortical bone) are discontinuously represented in the *Publication* 110 phantoms (ICRP, 2009; Yeom et al., 2013; Yeom et al., 2016b), whereas those are continuously represented in the MRCPs.

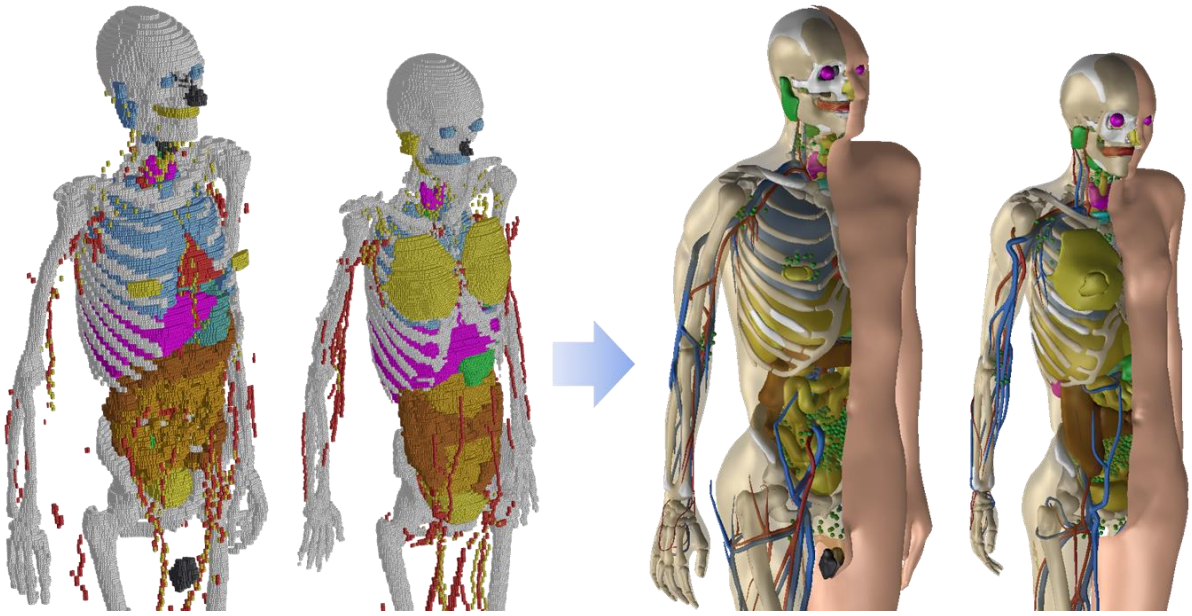

Fig. 4. The adult mesh-type reference phantoms (right), along with the voxel-type *Publication* 110 reference phantoms (left).

3. COMPATIBLITY WITH MONTE CARLO CODES

The major Monte Carlo radiation transport codes, such as Geant4, MCNP6, PHITS and FLUKA, can directly implement polygon-mesh (PM) or tetrahedron-mesh (TM) geometries The Geant4 code can implements both PM and TM geometries by using *G4TessellatedSolid* class and *G4Tet* class, respectively (Agostinelli et al., 2003). The MCNP6 code, as a merger of MCNP5 and MCNPX capabilities, provides the unstructured mesh geometry which can implement the TM geometries. Note that since the version 1.1 beta of the MCNP6, the unstructured mesh geometry can support the transport of most particles available in the MCNP6 code (Goorley et al., 2013), whereas in the previous version (i.e. ver. 1.0), the transport of only neutron and gamma was supported (Martz et al., 2012). The PHITS code, since the version 2.82, can implement TM geometries (Sato et al., 2013). Note that nowadays, mostly the PHITS code is used within ICRP to calculate dose coefficients (DCs). The FLUKA code can implement the PM geometry via FluDAG (http://svalinn.github.io/DAGMC/index.html).

Memory usage and computation speed were measured for Geant4 (ver. 10.03 patch01), MCNP6 (ver. 2.0 pre-release) and PHITS (ver. 2.92) when the male MRCP in the TM format was used in Monte Carlo dose calculation. For this, the MRCP was directly implemented into the Monte Carlo codes as shown in Fig. 5. The phantom was then irradiated in the isotropic (ISO) irradiation geometry. The considered primary particles are photons (10^{-2}–10^{4} MeV), electrons (10^{-2}–10^{4} MeV), neutrons (10^{-8}–10^{4} MeV) and helium ions (1–10^{5} MeV/u). To evaluate the computation speed, the computation time was measured by simulating 10^{5} primary particles. For the Geant4 code, the physics libraries of the *G4EmLivermorePhysics* and the *FTFP_BERT_HP* were used to transport all the particles. In addition, the thermal neutron scattering treatment S(α, β) for H in light water at 300 K was applied for precise transport of thermal neutrons. A default range of 1 mm for the secondary production cut was applied to all the particles. For both the MCNP6 code and the PHITS code, the default physics models and cross-section data were used to transport all the particles, and the thermal neutron scattering treatment was also applied. For the MCNP6 code, the default cut energies

were used, which were also applied to set cut energies for the PHITS code. The simulations were performed on a single core of Intel® Xeon® CPU E5-2698 v4 (@ 2.20 GHz CPU processors and 512 GB memory).

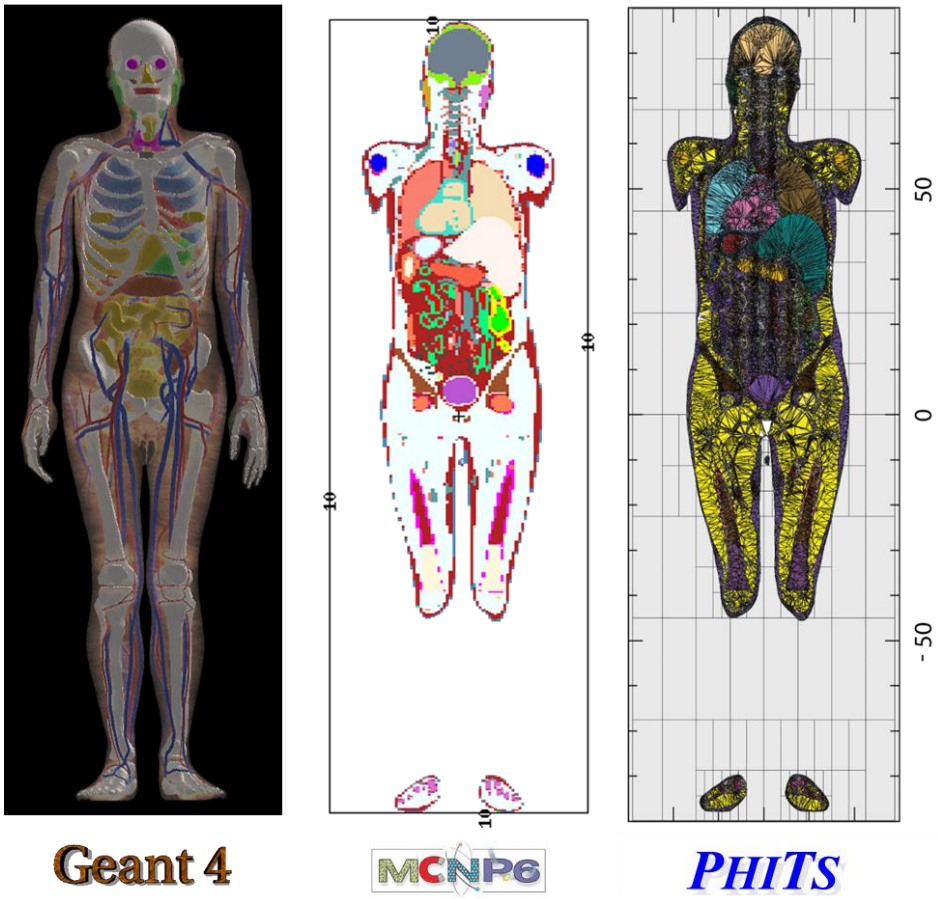

Fig. 5. The adult male mesh-type reference computational phantom implemented in Geant4 (left), PHITS (middle) and MCNP6 (right).

First, memory usage was measured for the three Monte Carlo codes. The Geant4 code required ~11 GB, which is slightly smaller than that required in the MCNP6 code (~14 GB). The PHITS code, when compared to the other codes, required much less memory, i.e. ~1.2 GB, which is because the PHITS uses dynamic allocation for most of the memory needed for implementing the MRCP. Considering the memory usages, all of the Monte Carlo codes can be used for dose calculations with the MRCPs in a personal computer, equipping 64 GB at maximum. In addition, initialization times were measured for the three Monte Carlo codes, which were all less than a few minutes, negligibly contributing to the total computation time in typical dose coefficient calculations requiring several hours or to tens of hours depending on particles and energies (Furuta et al., 2017).

Computation speed of the MRCP on the three Monte Carlo codes was measured and then compared with that measured with the *Publication* 110 male phantom on the PHITS code. Again note that nowadays, within the ICRP, most of the dose coefficients (DCs) are calculated by using the *Publication* 110 phantoms and the PHITS code. Fig. 6 shows the relative computation speed of the adult male MRCP on the three Monte Carlo codes, with respect to the computation speed of the *Publication* 110 phantom on the PHITS code (= the ratio of the MRCP computation speed on the Monte Carlo codes to the computation speed of the *Publication* 110 phantom on the PHITS code). First of all, it can be seen that the relative computation speed of the MRCP on the PHITS code is generally greater than unity, which

means that the computation speed of the MRCP is generally faster than that of the *Publication* 110 phantom on the PHITS code. This result is very encouraging and implies that, assuming that the ICRP keeps using the PHITS code for most DC calculations, the use of MRCPs will even improve the computation speed of DCs. For the Geant4 code, the computation speed of the MRCP is faster or comparable to that of the *Publication* 110 phantom on the PHITS code for photons, electrons, and helium ions. For neutrons, however, with only an exception at 10^4 MeV, the computation speed of the MRCP is much slower, i.e. by more than 30 times at 1 MeV. For the MCNP6 code, for all the considered cases, the computation speed of the MRCP is much slower than that of the *Publication* 110 phantom on the PHITS code, i.e. by a factor of 2–22. This seems mainly due to the fact that the MCNP6 code uses the unstructured mesh geometry, which is very flexible but overly sophisticated to define the simple tetrahedral-mesh geometry. We believe that the computation speed will improve if the MCNP6 code uses a dedicated geometry for tetrahedral-mesh geometry in the future.

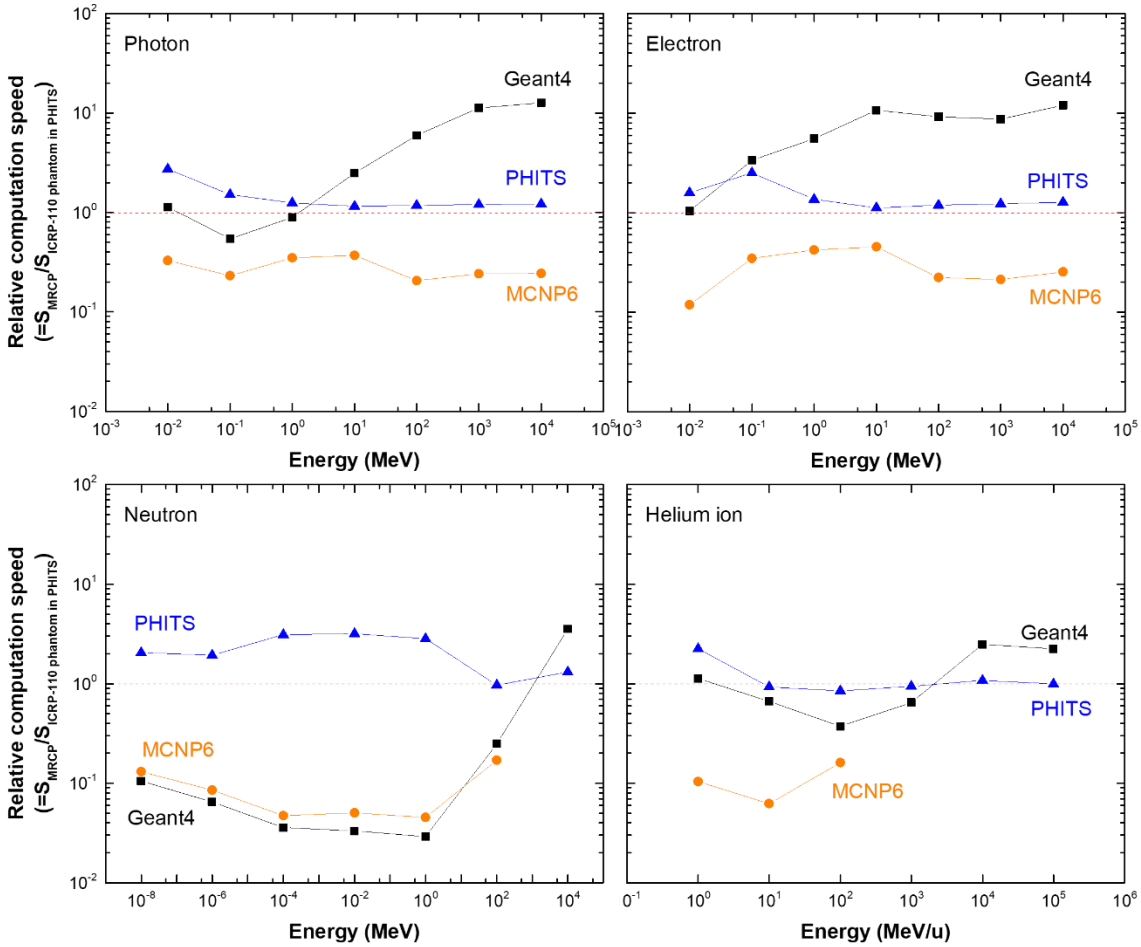

Fig. 6. Relative computation speed of the adult male MRCP on Geant4, PHITS and MCNP6, with respect to the computation speed of the *Publication* 110 male phantom on the PHITS code.

4. COMPARISON OF DOSE COEFFICIENTS

In order to evaluate the impact of the adult MRCPs in dose calculations, dose coefficients (DCs) were calculated for some selected external and internal exposure geometries and the calculated DCs were then compared with the reference values of *Publications* 116 and 133 (ICRP, 2010, 2016) that were evaluated by using the *Publication* 110 (ICRP, 2009) phantoms

and the stylised models described in *Publications* (ICRP, 1994, 2006, 2015, 2016, 2017). For the purpose of these calculations, the MRCPs were directly implemented into the Geant4 code. Similar to the calculations of the computation speeds, the physics libraries of the *G4EmLivermorePhysics* and the *FTFP_BERT_HP* were used with the thermal neutron scattering treatment, but the default range of 1 mm for the secondary production cut was changed to 1 μm for more precise dose calculations. For external exposures, the effective dose coefficients (DCs) in terms of effective dose per fluence (in pSv cm^2) were calculated for monoenergetic broad parallel beams of photons, neutrons, electrons and helium ions for the same irradiation geometries considered in *Publication* 116 (ICRP, 2010). For internal exposures, the effective doses per radiation emission (EDREs) for photons and electrons were calculated for selected source organs/tissues: the cortical bone, liver, lungs and thyroid. Note that the EDRE is the expectation value of the effective dose resulting from an emission of a single radiation particle in a source organ/tissue, which is calculated from specific absorbed fractions (SAFs) and the radiation and tissue weighting factors of *Publication* 103 (ICRP, 2007). The statistical errors of the calculated values were all less than 0.5%.

The calculation results showed that for the photons and neutrons, the MRCPs tended to provide very similar DC values for both organ/tissue doses and effective doses to the reference values in *Publications* 116 and 133 for both external and internal exposures. The differences in the effective doses, the most important protection quantity, were even smaller than those in the organ/tissue doses. For photons, for example, with some exceptions at low energies (< 0.03 MeV), the effective dose differences were less than 2% for external exposures and less than 5% for internal exposures. For neutrons, the differences were larger due to the different Monte Carlo codes used in the calculations, but still less than 10% for most external exposure cases. Note that the *Publication* 116 values were calculated using several different codes such as MCNPX, PHITS, FLUKA, EGSnrc Geant4 and the reference values were derived by averaging and smoothing tequniques (ICRP, 2010). For charged particles (i.e. electrons and helium ions), in contrast, the MRCPs tended to provide different values from the *Publications* 116 and 133 values for the organ/tissue DCs and SAFs, for both external and internal exposures. For the effective doses, however, with some exceptions, the differences were generally not very large, i.e. less than ~5% for most cases for both external and internal exposures.

Exceptions were observed in the results of external exposures by electrons (< 1 MeV) and by helium ions (< 10 MeV/u). Fig. 7 shows an example of the effective DCs for electron exposures in the antero-posterior (AP) irradiation geometry. It can be seen that the effective DCs of the MRCPs are very similar to the *Publication* 116 values for the energies higher than 1 MeV, but for the lower energies, there are larger differences; the maximum difference is as large as ~7000 times at the lowest energy. These differences are mostly due to the differences of the skin DCs, which are mainly caused by the use of the 50-μm-thick skin target layer in the MRCPs rather than the one-voxel thickness of 2.137 and 1.775 mm for the male and female phantom respectively, representing the skin thickness of these phantoms The same level of differences were also found in the results for other irradiation geometries.

However, the differences could be overly exaggerated when considering monoenergetic electron beams; in real exposure situations, generally polyenergetic electrons (e.g. beta spectra) are involved, where the difference in effective doses is less significant. For example, the difference of effective dose between the MRCPs and the *Publication* 110 phantoms resulting from the AP irradiation of the beta radiation sources (^{14}C, ^{186}Re, ^{32}P, $^{90}Sr/^{90}Y$ and ^{106}Rh) is less than ~2 times, except for ^{14}C, for which the difference is ~5 times. Note that ^{14}C emits very low energy electrons (0.15 MeV maximum) and thus is generally not of concern for external exposures.

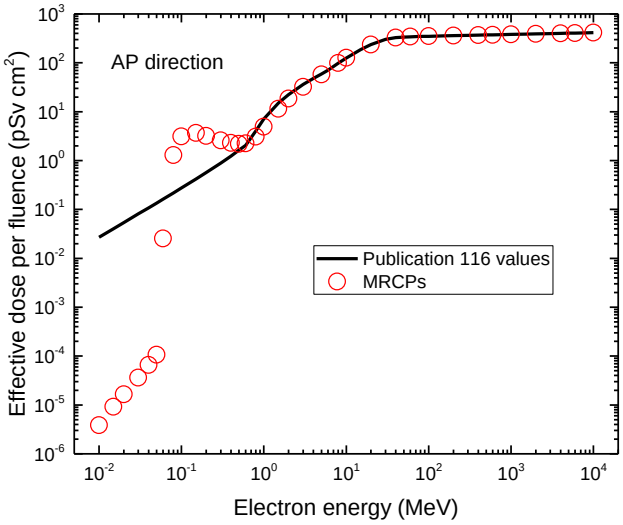

Fig. 7. Effective dose per fluence (pSv cm^2) for monoenergetic electrons and isotropic (ISO) irradiation geometry calculated with the adult MRCPs (red circles); also shown the *Publication* 116 values (black line).

5. CALCULATION OF DOSE COEFFICIENTS FOR INDUSTRIAL RADIOGRAPHY SOURCES

Using the adult MRCPs, Task Group 103 is currently calculating dose coefficients (DCs) for industrial radiography sources, which can be used to estimate organ/tissue and effective doses of workers who are accidentally exposed by an industrial radiography source. According to IAEA (2011), accidents involving industrial radiography sources result in very high radiation doses to workers, causing serious injuries and, in a few cases, even death. IAEA (1998) also states that industrial radiography accounts for approximately half of all the reported accidents for the nuclear related industry, in both developed and developing countries.

For the DC calculations, ^{192}Ir and ^{60}Co industrial radiography sources were assumed as a point source and modelled near the MRCPs. The point sources are located at three distances (0.5, 10 and 30 cm) in four directions (front, back, right and left) at five levels (ground, middle thigh and lower, middle and upper torso) (see Fig. 8). In addition, three longer distances (100, 150 and 300 cm) are considered in the four directions at the lower torso level. The source distance used in the calculations is the distance from the surface of the phantom, except for the front and back directions at the ground and middle thigh levels, for which the distance is calculated from the centre of the imaginary segment tangent to the surfaces of the left and right legs at the given level. Organ/tissue DCs (= absorbed dose per disintegration) for red bone marrow (RBM), brain, lungs and small and large intestines are calculated, considering acute radiation syndromes. Effective DCs (= effective dose per disintegration) are additionally calculated for comparison purpose.

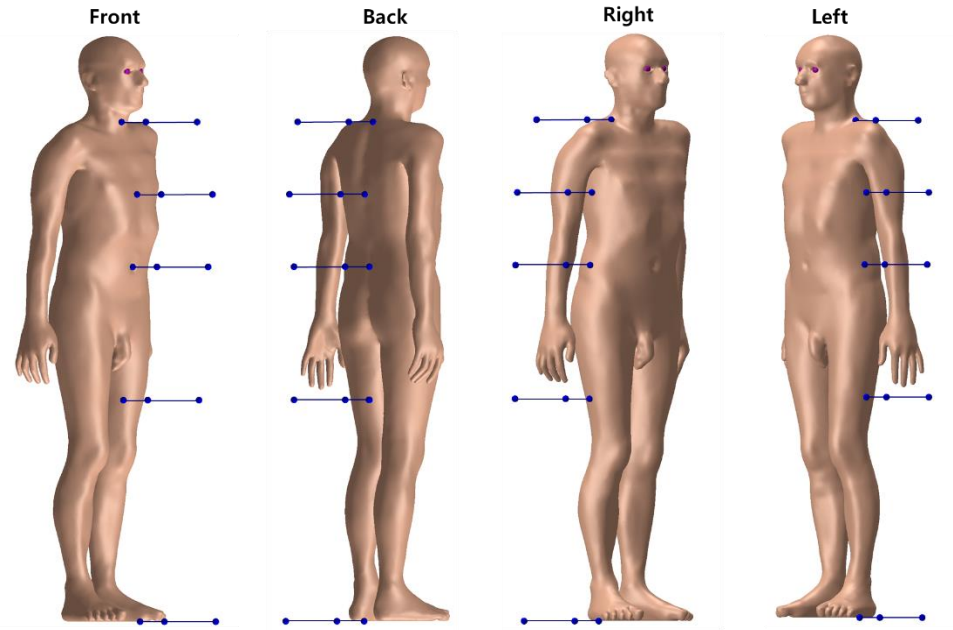

Fig. 8. Source locations at three distances (0.5, 10 and 30 cm) at five levels (ground, middle thigh and lower, middle and upper torso) in four directions (front, back, right and left).

In addition to the MRCPs, the 10th and 90th percentile phantoms are also employed in the DC calculations to consider the influence of different body sizes on DCs. Fig. 9 shows the 10th and 90th percentile male phantoms, along with the adult male MRCP. The 10th percentile phantom, which represents a very small person, was constructed by reducing the size of the MRCPs to the 10th percentile standing height and 10th percentile body mass in the Caucasian population. In contrast, the 90th percentile phantom, which represents a very large person, was constructed by increasing the size of the MRCPs to the 90th percentile standing height and 90th percentile body mass. For the constructions, the standing height and body mass percentiles were derived from the data of the nine countries (i.e. Sweden, Netherlands, Germany, Belgium, Australia, USA, France, UK and Italy) provided in the PeopleSize commercial software (www.openerg.com). Additional anthropometric parameters (i.e. head height, length and breadth, upper arm, waist, buttock, thigh and calf circumferences, waist depth, and sitting height), corresponding to the standing height and body mass percentiles, were derived not only from the PeopleSize data but also from the National Health and Nutrition Examination Survey (NHANES) (https://www.cdc.gov/nchs/nhanes/index.htm) and the US Army Anthropometric Survey (ANSUR II) (Gordon et al., 2014) databases. A complete set of the DCs of the MRCPs and the 10th and 90th percentile phantoms will be provided in the Task Group 103 report for the adult MRCPs. Additionally, the effect of different postures will be investigated by calculating DCs with several phantoms with different postures (i.e. walking, sitting, bending, kneeling and squatting postures), which are now under construction by deforming the MRCPs. For the investigation, the DCs will be calculated for the lowest-energy source, ^{192}Ir, located at 100 cm from the phantom surface in the four directions at the lower torso level.

Fig. 10 shows, as an example, the small intestine DCs of the adult male MRCP, along with those of the 10th and 90th percentile adult male phantoms, for the ^{192}Ir source located in the four directions at the lower torso level. It can be seen that the body size indeed significantly influences the DC values. The DC of the 90th percentile phantom is smaller than that of the MRCP by up to 2.6 times (at 0.5 cm in the front direction). On the other hand, the DC of the 10th percentile phantom is larger by up to ~40% (at 0.5 cm in the front direction).

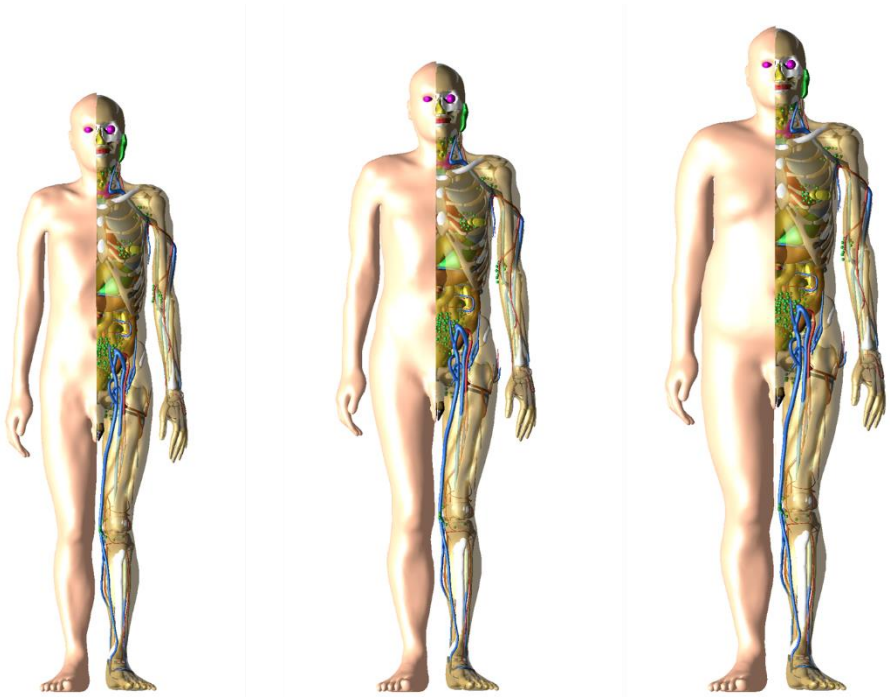

Fig. 9. Computational phantoms: 10th percentile phantom (left), MRCP (middle) and 90th percentile phantom for adult males.

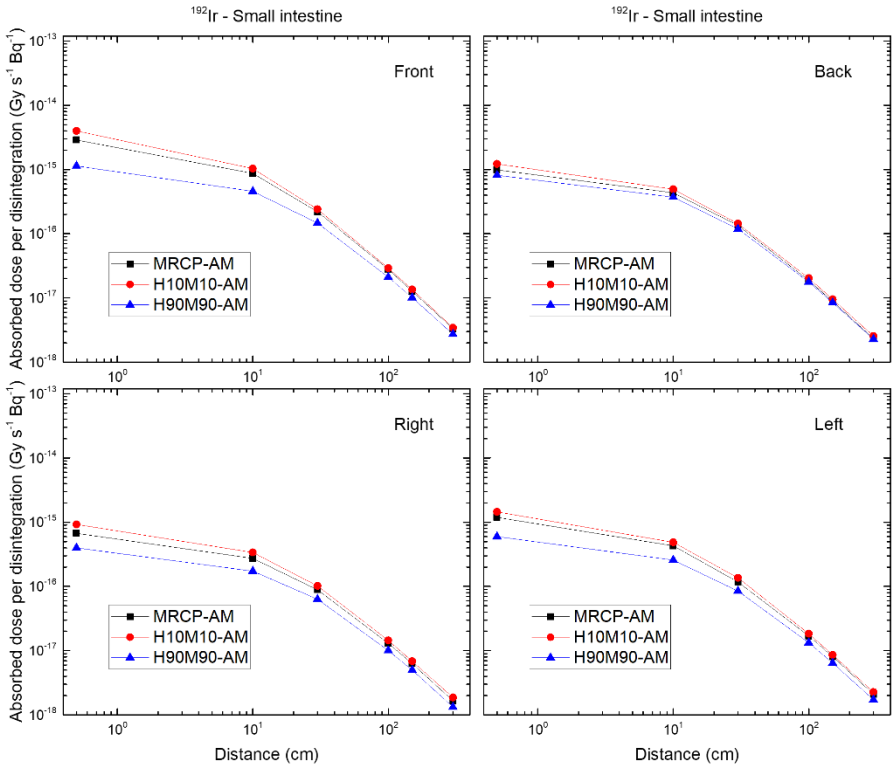

Fig. 10. Small intestine DCs of the adult male MRCP (black squares) for a point source of ^{192}Ir as a function of the distance from the surface of the phantom in the four directions (front, back, right and left) at the lower torso level, along with those of the 10th percentile adult male phantom (red circles) and 90th percentile adult male phantom (blue triangles).

6. CONCLUSIONS

Task Group 103 under Committee 2 has completed the construction of the adult male and female mesh-type reference computational phantoms (MRCPs), based on the reference phantoms of ICRP *Publication* 110, to provide a more flexible phantom format regarding size, posture and movement and containing stylized-type parts describing the very small tissues The adult MRCPs were constructed by converting the *Publication* 110 phantoms into a high-quality mesh format, also including all the necessary source and target tissues for effective dose calculations (e.g. the 8–40-μm-thick target layers of the alimentary and respiratory tract organs), thereby obviating the need for supplemental stylised models (e.g. respiratory airways, alimentary tract organ walls and stem cell layers, lens of the eye and skin basal layer). Furthermore, the compatibility of the MRCPs with three major general-purpose Monte Carlo codes (Geant4, PHITS and MCNP6) was investigated by measuring memory usage and computation speed; it was found that PHITS runs faster when coupled to the MRCPs than to the *Publication* 110 phantoms. The dosimetric impact of the MRCPs was also investigated by calculating dose coefficients (DCs) for some selected external and internal geometries, which were then compared with the reference values of *Publications* 116 and 133; the results showed that the MRCPs tend to provide very similar DC values for highly penetrating radiations (e.g. photons and neutrons), while providing more reliable DC values for weakly penetrating radiations (e.g. electrons and helium ions). In addition, Task Group 103 is currently calculating the DCs for industrial radiography sources; in these calculations, the MRCPs are deformed to reflect the size of individuals and also to evaluate the effect of the posture on DCs, which demonstrates the capability of the MRCPs in individualized dose calculations. Acknowledging the advantages, Committee 2 is planning to use the MRCPs in calculation of dose coefficients for emergency exposure situations, which is planned for the next term (2017-2020). The Task Group 103 report is now under preparation in order to officially release the adult MRCPs; the report is expected to be published in 2019, after public consultation in 2018.

REFERENCES

Agostinelli S., et al., 2003. GEANT4—a simulation toolkit. Nucl. Instrum. Methods Phys. Res. A, 506 250–303

Apostolakis J., et al., 2008. Parallel geometries in Geant4: foundation and recent enhancements IEEE Nucl. Sci. Symp. Conf. Record (NSS ‘08) 883–886

Behrens R., Dietze G., Zankl M., 2009. Dose conversion coefficients for electron exposure of the human eye lens. Phys. Med. Biol. 54 4069–87

Dice L., 1945. Measures of the amount of ecologic association between species Ecology 26 297–302

Furuta, T., Sato, T., Han, M,C., et al., 2017. Implementation of tetrahedral-mesh geometry in Monte Carlo radiation transport code PHITS. Phys. Med. Biol. 62, 4798–4810

Goorley, J.T., et al., 2013. Initial MCNP6 release overview-MCNP6 version 1.0. Los Alamos National Laboratory, Los Alamos, NM, LA-UR-13-22934.

Gordon, C.C., Blackwell, C.L., Bradtmiller, B., et al., 2014 2012 Anthropometric Survey of U.S. Army Personnel: Methods and Summary Statistics. NATICK/TR-15/007. Natick, MA: U.S. Army Natick Soldier Research, Development, and Engineering Center.

Han M. C., Kim C. H., Jeong J. H., et al., 2013 DagSolid: a new Geant4 solid class for fast simulation in polygon-mesh geometry. Phys. Med. Biol. **58** 4595–4609

Han M. C., Yeom Y. S., Kim C. H., et al., 2015 New approach based on tetrahedral-mesh geometry for accurate 4D Monte Carlo patient-dose calculation. Phys. Med. Biol. **60** 1601–1612

IAEA. SAFETY STANDARDS SERIES No. SSG-11 Radiation Safety in Industrial Radiography. Vienna, 2011.

IAEA. Lessons learned from accidents in industrial radiography. Safety Reports Series, No. 7. Vienna, 1998.

ICRP, 1977. Recommendations of the ICRP. ICRP Publication 26. Ann. ICRP 1 (3).

ICRP, 1994. Human Respiratory Tract Model for Radiological Protection. ICRP Publication 66. Ann. ICRP 24 (1-3).

ICRP, 2002. Basic Anatomical and Physiological Data for Use in Radiological Protection Reference Values. ICRP Publication 89. Ann. ICRP 32 (3-4).

ICRP, 2006. Human Alimentary Tract Model for Radiological Protection. ICRP Publication 100. Ann. ICRP 36 (1-2).

ICRP, 2007. The 2007 Recommendations of the International Commission on Radiological Protection. ICRP Publication 103. Ann. ICRP 37 (2-4).

ICRP, 2009. Adult Reference Computational Phantoms. ICRP Publication 110. Ann. ICRP 39 (2).

ICRP, 2010. Conversion Coefficients for Radiological Protection Quantities for External Radiation Exposures. ICRP Publication 116, Ann. ICRP 40 (2-5).

ICRP, 2015. Occupational Intakes of Radionuclides: Part 1. ICRP Publication 130. Ann. ICRP 44(2).

ICRP, 2016. The ICRP computational framework for internal dose assessment for reference adults: specific absorbed fractions. ICRP Publication 133. Ann. ICRP 45(2), 1−74.

ICRP, 2017. Occupational Intakes of Radionuclides: Part 2. ICRP Publication 134. Ann. ICRP 45(3/4), 1–352.

Kim, C.H., Jeong, J.H., Bolch, W., et al., 2011. A polygon-surface reference Korean male phantom (PSRK-Man) and its direct implementation in Geant4 Monte Carlo simulation. Phys. Med. Biol. 56, 3137–3161

Kim, C.H., Yeom, Y.S., Nguyen, T.T., et al., 2016. The reference phantoms: voxel vs polygon. Ann. ICRP 45(1S), 188–201.

Kim H. S., Yeom Y. S., Nguyen T. T., et al., 2017. Inclusion of thin target and source regions in alimentary and respiratory tract systems of mesh-type ICRP adult reference phantoms. Phys. Med. Biol. 62, 2132–2152

Kramer R, Khoury H J, Vieira J W and Lima V J M 2006 MAX06 and FAX06: update of two adult human phantoms for radiation protection dosimetry Phys. Med. Biol. 51 3331–46

Kramer, R., Zankl, M., Williams, G., et al., 1982. The calculation of dose from external photon exposures using reference human phantoms and Monte Carlo methods, Part I: The male (Adam) and female (Eva) adult mathematical phantoms. GSF-Report S-885, GSF - National Research Center for Environment and Health, Neuherberg, Germany.

Lee C., Lodwick D., Hurtado J., et al., 2010. The UF family of reference hybrid phantoms for computational radiation dosimetry. Phys. Med. Biol. 55, 339–363

Lee C., Lamart S., Moroz B. E., 2013. Computational lymphatic node models in pediatric and adult hybrid phantoms for radiation dosimetry. Phys. Med. Biol. 58 N59–N82

Lee C., Lodwick D., Hasenauer D., et al., 2007. Hybrid computational phantoms of the male and female newborn patient: NURBS-based whole-body models. Phys. Med. Biol. 52 3309-3333

Martz, R., The MCNP6 Book on Unstructured Mesh Geometry: User′s Guide. Los Alamos National Laboratory, Los Alamos, NM, (2012).

Nguyen T. T., Yeom Y. S., Kim H. S., et al., 2015. Incorporation of detailed eye model into polygon-mesh versions of ICRP-110 reference phantoms. Phys. Med. Biol. 60 8695–8707

Sato T., Niita K., Matsuda N., et al., 2013. Particle and Heavy Ion Transport Code System PHITS, Version 2.52, J. Nucl. Sci. Technol. 50 (9) 913-923

Si H., 2015. TetGen, a Delaunay-Based Quality Tetrahedral Mesh Generator. ACM Trans. on Mathematical Software. 41 (2), Article 11 (February 2015), 36 pages. DOI=10.1145/2629697 http://doi.acm.org/10.1145/262969

Tawhai M. H., Pullan A. J., Hunter P. J., 2000. Generation of an anatomically based three-dimensional model of the conducting airways Ann. Biomed. Eng. 28 793-802

Yeom Y. S., Han M. C., Kim C. H., et al., 2013. Conversion of ICRP male reference phantom to polygon-surface phantom. Phys. Med. Biol. 58, 6985–7007

Yeom, Y.S., Jeong J. H., Han M. C., et al., 2014. Tetrahedral-mesh based computational human phantom for fast Monte Carlo dose calculations. Phys. Med. Biol. 59, 3173-3185.

Yeom Y. S., Kim H. S., Nguyen T. T., et al., 2016a. New small-intestine modelling method for surface-based computational human phantoms. Journal of Radiological Protection 36, 230–245

Yeom Y. S., Wang Z. J., Nguyen T. T., et al., 2016b. Development of skeletal system for mesh-type ICRP reference adult phantoms. Phys. Med. Biol. 61, 7054–7073

Zankl, M., Becker, J., Fill, U., et al., 2005. GSF male and female adult voxel models representing ICRP Reference Man – the present status. In: The Monte Carlo Method: Versatility Unbounded in a Dynamic Computing World. American Nuclear Society, LaGrange Park, IL

Zhang J, Na Y H, Caracappa P F, Xu X G 2009 RPI-AM and RPI-AF, a pair of mesh-based, size adjustable adult male and female computational phantoms using ICRP-89 parameters and their calculations for organ doses from monoenergetic photon beams. Phys. Med. Biol. 54 5885–908